Thermoviscoelastic shape memory behavior for epoxy-shape memory polymer

2014 Smart Mater. Struct. 23 055025

(http://iopscience.iop.org/0964-1726/23/5/055025)

IOP Publishing Smart Materials and Structures
Smart Mater. Struct. **23** (2014) 055025 (14pp) doi:10.1088/0964-1726/23/5/055025

Thermoviscoelastic shape memory behavior for epoxy-shape memory polymer

Jianguo Chen[1], Liwu Liu[1], Yanju Liu[1] and Jinsong Leng[2]

[1] Department of Astronautical Science and Mechanics, Harbin Institute of Technology (HIT), PO Box 301, No 92 West Dazhi Street, Harbin 150001, People's Republic of China
[2] Centre for Composite Materials, Science Park of Harbin Institute of Technology (HIT), PO Box 3011, No 2 YiKuang Street, Harbin 150080, People's Republic of China

E-mail: yj_liu@hit.edu.cn and lengjs@hit.edu.cn

Received 16 December 2013, revised 28 January 2014
Accepted for publication 24 February 2014
Published 1 April 2014

Abstract

There are various applications for shape memory polymer (SMP) in the smart materials and structures field due to its large recoverable strain and controllable driving method. The mechanical shape memory deformation mechanism is so obscure that many samples and test schemes have to be tried in order to verify a final design proposal for a smart structure system. This paper proposes a simple and very useful method to unambiguously analyze the thermoviscoelastic shape memory behavior of SMP smart structures. First, experiments under different temperature and loading conditions are performed to characterize the large deformation and thermoviscoelastic behavior of epoxy-SMP. Then, a rheological constitutive model, which is composed of a revised standard linear solid (SLS) element and a thermal expansion element, is proposed for epoxy-SMP. The thermomechanical coupling effect and nonlinear viscous flowing rules are considered in the model. Then, the model is used to predict the measured rubbery and time-dependent response of the material, and different thermomechanical loading histories are adopted to verify the shape memory behavior of the model. The results of the calculation agree with experiments satisfactorily. The proposed shape memory model is practical for the design of SMP smart structures.

Keywords: shape memory polymer, shape memory model, thermomechanical behavior, large deformation

(Some figures may appear in colour only in the online journal)

1. Introduction

Shape memory polymer (SMP) and its composite structure system is becoming a new research direction in the smart materials and structures field [1–15]. As a kind of smart active deformation material, shape memory polymer has many advantages such as its obvious shape memory effect, large recoverable strain (up to 400%), controllable driving method, flexible design of the glass transition temperature, etc [4–6]. There are various applications for SMP in smart material and structure systems such as space deployable devices, bio-medical devices, textile products, sensors, etc [7–11].

Shape memory polymer is a special kind of polymer which can perceive external stimulus (such as heat [12, 13], magnetism [14, 15], light [16–19], electricity [20–22], etc). The material has certain shape memory effects. If it is given a load under certain conditions, the material can alter its shape and fix it thereafter if the external environment changes; the material can then perfectly recover to its initial shape if the external conditions change back to their original state. This 'remember initial shape–fix deformation state–recover to original shape' cycle is called the shape memory effect (SME) [23–26]. Using thermal active SMP as an example, when heated to above the glass transition temperature T_g

the material can be deformed under external force; then the temperature is reduced to below the glass transition while keeping the external force applied; and then the external force is unloaded and the given shape is kept; when heated to above the glass transition temperature again the SMP can recover to its initial shape automatically [1, 7].

Shape memory polymer has been researched for over twenty years, and has gradually become more widely used because of its unique advantages over other smart materials. The mechanical shape memory deformation mechanism is so obscure that many samples and test schemes have to be tried in order to verify a final design proposal for a smart structure system.

Thermal active SMP, in particular epoxy-SMP, is the main focus of this paper. The shape memory effect of thermal active SMP can be described by the three-dimensional thermomechanical cycle of stress–strain–temperature. There is some research work on the shape memory behavior of SMP, but it is not definitive. Tobushi, as early as 1997, introduced a slip friction unit into the traditional linear viscoelastic three-unit model to describe the freezing strain of the SMP material based on linear viscoelastic theory and systematically studied the constitutive behavior of shape memory polyurethane, establishing a four-unit phenomenological thermodynamic constitutive equation [27]. In order to describe the constitutive relation of the material under large strain conditions, Tobushi, in 2001, revised the linear model by proposing a nonlinear deformation model [28]. Using this model, Tobushi obtained the stress–strain and stress–temperature relationships at 20% strain level, and the results agreed with experiments, indicating that the model was suitable for shape memory polyurethane materials. However, this model is just one-dimensional and the slip friction unit is very confusing. On the other hand, Liu *et al* developed a two-phase transition microstructure constitutive model of shape memory polymer [29]. The model defined two internal state parameters in shape memory polymer: the frozen phase and the active phase. The frozen phase is the freezing part of the material in the cooling process, with the assumption that the frozen phase and active phase inherit the same stress. On this basis, a three-dimensional, linear elastic, small deformation rate independent constitutive model was proposed. Based on the transition mechanism proposition between the frozen phase and the active phase proposed by Liu, Chen and Lagoudas developed a nonlinear constitutive model. The model further described the stress recovery and strain storage mechanism in the shape recovery process of the thermomechanical cycle [30, 31]. The theoretical predictions of the model complied with experimental results by Liu [29]. Based on the phase transition theory, Barot and Rao also carried out some further research [32]. In addition, Qi also put forward a new constitutive model of SMP. The model was a 3D finite deformation model which assumed that the material has three-phase structure: the rubbery phase (RP), the initial glassy phase (IGP) and the frozen glassy phase (FGP) [33]. The advantage of this model is that there is no use of the concept 'storage strain' in the model and the model is not confined to elastomeric polymer or vitreous polymer modeling—it can be used for modeling of any other material that has an SME. This model is more accurate than that of Liu for simulation of the material property changes in the high-temperature to low-temperature cooling process [29]. Kai Yu investigated the underlying physical mechanisms for the observed multi-shape memory behavior and the associated energy storage and release by using a theoretical modeling approach [34]. Qi Ge developed a simple theoretical solution which is based on a modified standard linear solid (SLS) model with a Kohlrausch–Williams–Watts (KWW) stretched exponential function to predict the temperature-dependent free recovery behavior of amorphous SMPs [35]. Kai Yu also reported a unified approach to predict shape memory performance under different thermotemporal conditions such as the shape fixity and free recovery of thermorheologically simple shape memory polymers [36]. There are some other models to characterize the mechanical behavior of SMP, but almost all of them are very complex and need too many model parameters, and many model parameters do not have any physical meaning [37, 38]. Moreover, due to high modulus of SMP in the glassy state, the release of stress is significantly affected by the thermal expansion of the polymer, which then leads to creep and stress relaxation, which are not considered well in many works.

As described above, various thermomechanical transitions such as the glass transition or melting transition can be utilized for shape memory modeling. For polymers using the glass transition to achieve shape memory, the underlying physical mechanism of shape memory effects is the dramatic chain mobility (or relaxation time) change as the temperature traverses the glass transition temperature (T_g).

This work focuses on modeling the strain–stress–temperature response of epoxy-SMP. Using the framework of multiplicative decomposition of the deformation gradient, a rheological model based on a revised standard linear solid (SLS) element and a thermal expansion element is employed to develop a nonlinear viscoelastic finite strain constitutive model. Guided by similar developments in the area of the elasticity model for glassy and rubbery polymers, the rubbery response of the material is represented by the Mooney–Rivlin energy function and the high stiffness of the glassy state is modeled using Hencky's strain energy function. All experiments are carried out from the virgin state of the material. After all experiments have been presented in section 2, the constitutive model is detailed in section 3. The model parameters are identified in sections 4 and 5. A final discussion of the comparison of simulations and experimental results for epoxy-SMP is given in section 6.

2. Experimental investigation

2.1. Material

The epoxy-SMP used in this paper was synthesized and processed by Leng's research group [1, 7]. Uniaxial tensile test samples were cut following the standard ASTM-D638, Type IV. Samples 5.8 mm wide, 115 mm long, 2.5 mm thick and of gauge length 25 mm were machined using a laser cutting machine. The test specimens used in the DMA experiment were 1.8 mm × 4.8 mm × 18.5 mm. All experiments were performed on epoxy-SMP in its virgin state.

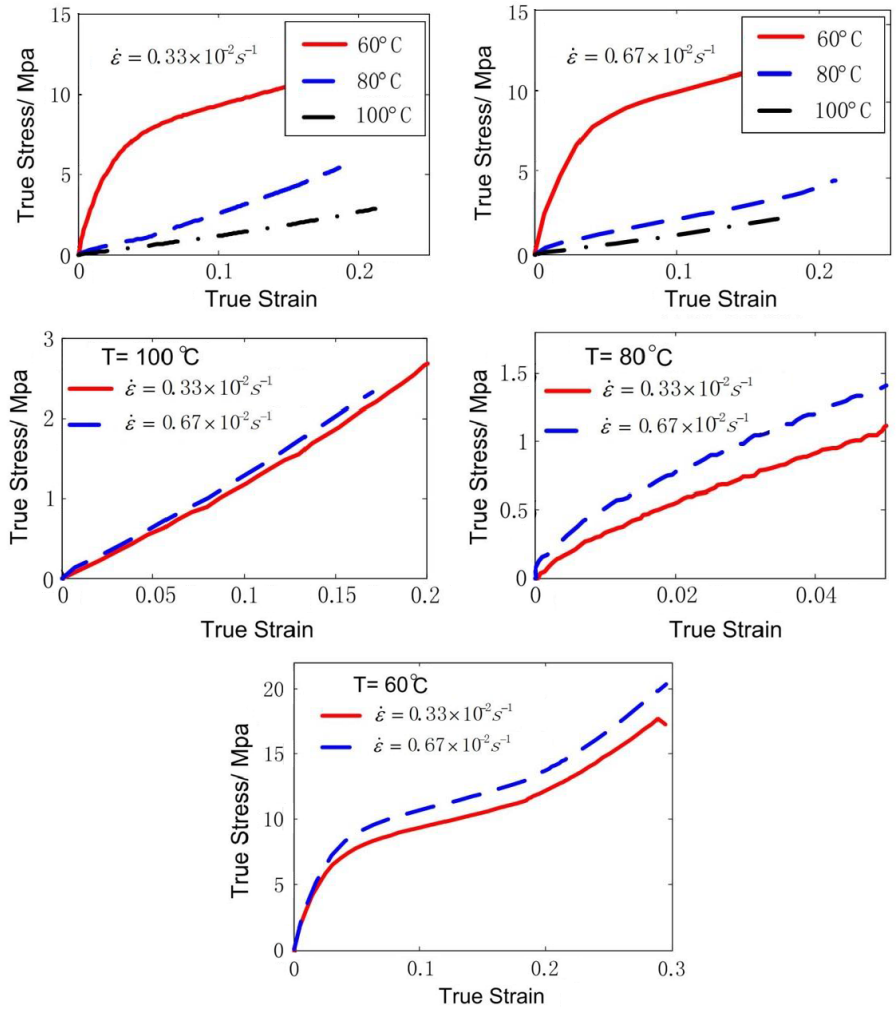

Figure 1. Uniaxial tensile experiments on epoxy-SMP. The temperature conditions are 60, 80 and 100 °C and the strain rates are 0.33×10^{-2} s^{-1} and 0.67×10^{-2} s^{-1}.

2.2. Isothermal uniaxial tensile experiments

When considering the effect of the temperature and strain rate on the mechanical performance of epoxy-SMP, the mechanical performance in the vicinity of the glass transition temperature is the primary concern. Isothermal tensile experiments were conducted using a Zwick/Roell test machine. An extensometer was used to measure the strain during the experiments, and a matched temperature control box provided the low- and high-temperature environments. Samples were pre-loaded to 0.1 MPa before the stress measurement to ensure good contact. The temperature conditions were set as 60, 80 and 100 °C, and two different strain rates (0.33×10^{-2} s^{-1} and 0.67×10^{-2} s^{-1}) were applied. The environmental temperature was controlled by the supporting program and the target temperature was held for 5 min before the start of the test.

The measured true stress versus logarithmic strain curves for two different strain rates are summarized in figure 1. The true stress and true strain are used in this paper without further description.

It can be seen that during the loading process, the observed stress level exhibits strong strain rate sensitivity. For example, the observed stress level for 0.33×10^{-2} s^{-1} is higher than that for 0.67×10^{-2} s^{-1} under the same temperature conditions. That is to say the modulus and the strength become higher when the applied strain rate increases. The observed stress level also exhibits strong temperature sensitivity; for example, the observed stress level for 100 °C is lower than that for 60 °C under the same strain rate level. That is to say the elastic modulus and the strength of the epoxy-SMP become lower when the temperature increases. Note that a yielding effect can be detected in the tensile test below the glass transition temperature of epoxy-SMP.

2.3. DMA experiments

Dynamic mechanical analysis (DMA) was used to study the viscoelastic properties of the material within a certain temperature range. The DMA test was performed to obtain the strain response of the material under low oscillation stress level, to study the thermomechanical properties (such as storage modulus, loss modulus, loss angle, etc) under different temperature conditions. The glass transition temperature T_g is defined as the peak temperature of the loss angle, which is the ratio of the storage modulus to loss modulus.

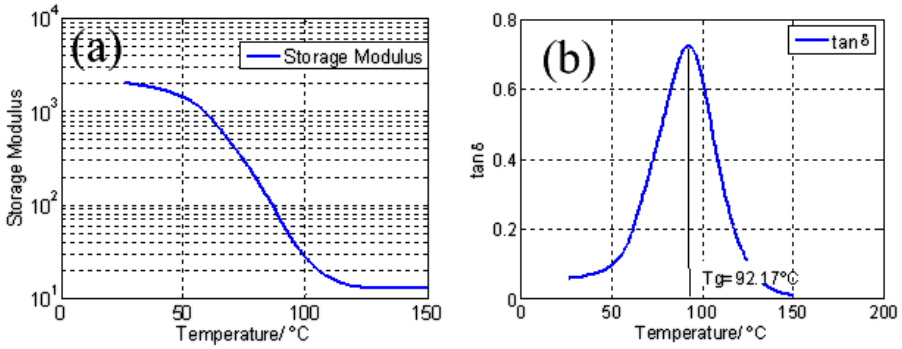

Figure 2. Storage modulus (a) and loss angle (b) of epoxy-SMP.

DMA tests were conducted using a Mettler Toledo Corporation DMA/SDTA861e machine to characterize the dynamic thermomechanical properties of epoxy-SMP. The tensile mode was used in the test, and a scanning temperature range from 25 to 250 °C. A small dynamic load at a frequency of 1 Hz was applied to the specimens and the rate of temperature rise was 5 °C min^{-1}.

As shown in figure 2, the glass transition temperature T_g of epoxy-SMP is 92.17 °C. In the low-temperature range 25–80 °C, the modulus is high and the material is in a glassy state; the material can be treated as a glassy material. In the mid-temperature range 80–120 °C, the modulus decreases sharply. In the high-temperature range 120–200 °C, the modulus is very low; the material becomes very soft and is in a rubbery state or even a flowing state if the temperature continues to increase, so the material can be treated as a rubbery material. Therefore, the glassy modulus of epoxy-SMP is 2.03 GPa (25 °C) and the rubbery modulus of epoxy-SMP is 13 MPa (120 °C).

2.4. Thermal expansion experiments

The coefficients of thermal expansion (CTE) were measured using a temperature control box and a laser displacement sensor. The test sample was 38.38 mm × 1.71 mm × 3.08 mm. The sample was gripped vertically at one top of the ends. The laser displacement sensor was placed directly under the sample. The temperature was increased from 50 to 120 °C at a rate of 1 °C min^{-1}. The change of the specimen's length was recorded. The experimental result is shown in figure 3.

The lope of the thermal strain is defined as the CTE. From the experiments we can conclude on some thermal expansion characteristics of the epoxy-SMP. Under low-temperature conditions, the material is hard, the modulus is high and the CTE is relatively smaller. While the CTE of the material becomes larger, the modulus is lower when the temperature continues to rise beyond the glass transition temperature. The CTE of the material has an apparent change in the vicinity of the glass transition temperature T_g. Therefore, we have to consider the thermal expansion strain in the constitutive model because the thermal strain is very obvious with respect to the test samples in the experiments.

The CTE of the glassy state was obtained to be $\alpha_g = 1.17 \times 10^{-4}$ °C^{-1} and the CTE of the rubbery state was obtained to be $\alpha_r = 2.35 \times 10^{-4}$ °C^{-1}.

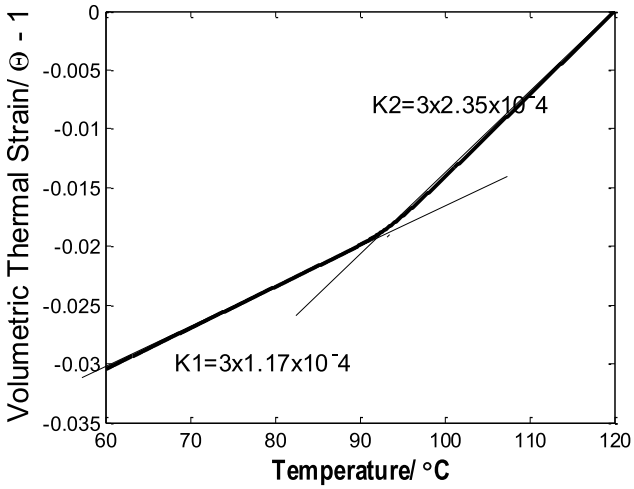

Figure 3. Thermal expansion performance of epoxy-SMP.

3. Constitutive theory of epoxy-SMP

3.1. Preview of the constitutive model

Thermoplastic epoxy-SMP exhibits a two-phase structure composed of a soft segment and a hard segment. The hard segment is responsible for the permanent shape, with a higher glass transition temperature (T_g), while the soft segment enables fixation of the temporary shape, with a lower T_g. During the shape memory cycle, the hard segment remains hard and provides the polymer with the shape-memorizing capability, while the soft segment softens upon heating above T_g or hardens on cooling below T_g and provides the elastic recovery properties of the polymer [33].

These segments are incompatible, which results in the formation of soft and hard domains. In the framework of multiplicative decomposition of the deformation gradient, and inspired by Qi and Boyce [39], we use a nonlinear spring element to represent the rate independent behavior of the soft domains, which is hyper-elastic, while a Maxwell element is used to describe the rate-dependent behavior of the hard part, which is viscoelastic. We call this two element form a revised standard linear solid (SLS) element. In addition, due to the apparent temperature dependence of the stress–strain curves, we use a thermal element to represent the thermal expansion effects (figure 4).

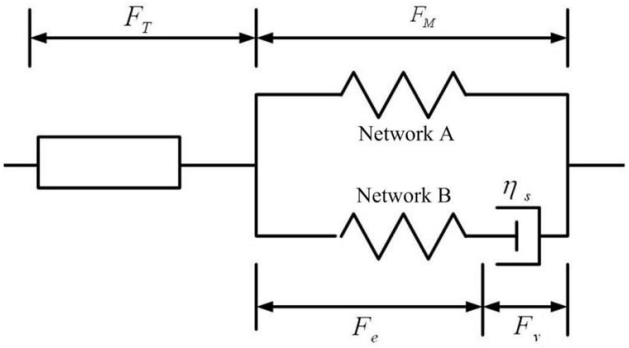

Figure 4. The proposed rheological constitutive model of epoxy-SMP.

The shape memory mechanism as illustrated in figure 4 makes the relationship between the thermal viscoelastic properties and the shape memory effect of the material sufficiently clear. The mechanical properties of the dashpot are characterized by its viscosity or relaxation time, which strongly depend on the temperature. As the temperature crosses the glass transition temperature, the viscosity can change dramatically. During a shape memory cycle, first, the material is deformed at a high temperature above T_g where the viscosity is very low. Therefore, the dashpot does not present much resistance to the deformation and thus develops a viscous strain close to the overall deformation of the material. As a result, the spring attached to the dashpot is in an almost undeformed state and the energy is stored mainly in the equilibrium branch. In the second step, the temperature is lowered to below T_g while the deformation is held constant. Decreasing the temperature below T_g leads to a dramatic increase of the viscosity in the dashpot. In the third step, the external load is removed. Because the viscosity is extremely high, the Maxwell element behaves like an elastic solid. Unloading will lead to elastic deformation of the springs in both the equilibrium and nonequilibrium branches due to the requirement of force balance. However, since the modulus of the spring in the Maxwell element is generally much higher than that of the spring in the equilibrium branch, the new deformation in the nonequilibrium branch is very small and much of the deformation introduced at the high temperature is fixed. Nonetheless, this causes an energy redistribution among the two springs. In the recovery step, the temperature is raised above T_g. As a result, the viscosity in the dashpot is dramatically decreased, the force in the spring attached to the dashpot drives the viscous strain back to zero, and the shape is recovered. Note that two features in the dashpot play an important role. First, it is the viscous strain that is frozen or memorized. Therefore, it is critical to allow the development of viscous strain during the programming step for the subsequent shape recovery behavior. Second, the dramatic change in viscosity is essential for the shape memory effect. When the viscosity is low, deformation of the material allows the development of a large viscous strain; in the subsequent cooling step, the viscosity becomes extremely high and thus the viscous strain developed at the high temperature is locked. During recovery, increase of the temperature reduces the viscosity and thus unlocks the viscous strain and recovers the shape.

The constitutive equations of the four basic elements of our rheological model are outlined in the following. Throughout the paper, we refer to the Maxwell element that is associated with the deformation resistance of the soft domain of the epoxy-SMP as 'network A', while the nonlinear spring element associated with the effect of the hard domain is referred to as 'network B'.

3.2. Total deformation and stress

The deformation gradient of the material is decomposed into the product of the thermal deformation gradient and the mechanical deformation gradient, while the mechanical deformation gradient is the further decomposition of the elastic deformation gradient and the viscous deformation gradient.

Suppose that any material point is at $\boldsymbol{X}$ before deformation (reference configuration), then is transformed to point $\boldsymbol{x}$ in the current configuration after the deformation under external force. The deformation gradient is defined as

$$\boldsymbol{F} = \partial \boldsymbol{x} / \partial \boldsymbol{X}. \tag{1}$$

The total deformation gradient $\boldsymbol{F}$ of the material is expressed as follows:

$$\boldsymbol{F} = \boldsymbol{F}_{\mathrm{M}} \boldsymbol{F}_{\mathrm{T}} = \boldsymbol{F}_{\mathrm{e}} \boldsymbol{F}_{\mathrm{v}} \boldsymbol{F}_{\mathrm{T}}, \tag{2}$$

where $\boldsymbol{F}_{\mathrm{M}}$ is the total mechanical deformation gradient, causing the change of stress; $\boldsymbol{F}_{\mathrm{T}}$ is the thermal deformation gradient, causing the thermal strain; $\boldsymbol{F}_{\mathrm{e}}$ is the elastic deformation gradient; and $\boldsymbol{F}_{\mathrm{v}}$ is the viscous deformation gradient.

The corresponding stress is the sum of the deviator stress caused by network A, the deviator stress caused by network B and the hydrostatic part due to mechanical volumetric deformation. The total Cauchy stress (true stress) of the material is

$$\boldsymbol{\sigma} = \bar{\boldsymbol{\sigma}}_{\mathrm{A}} + \bar{\boldsymbol{\sigma}}_{\mathrm{B}} + p\mathbf{1}, \tag{3}$$

where $\bar{\boldsymbol{\sigma}}_{\mathrm{A}}$ is the stress caused by the soft domain (or network A) and $\bar{\boldsymbol{\sigma}}_{\mathrm{B}}$ denotes the stress caused by the hard domain (or network B). p is the hydrostatic stress.

The volume change of epoxy-SMP under mechanical loading is very small compared with the thermal expansion and the isochoric deformation. We assume that the hydrostatic stress satisfies the following relationship:

$$p = \frac{1}{3}\boldsymbol{\sigma}_{kk} = k\frac{\ln J}{J}, \tag{4}$$

where k is the bulk modulus. $J = \det(\boldsymbol{F}_{\mathrm{M}})$ denotes the volumetric strain.

3.3. Thermal expansion

Suppose that the material is isotropic, then the thermal deformation gradient is

$$\boldsymbol{F}_{\mathrm{T}} = \Theta_{\mathrm{T}}^{1/3}\mathbf{1}, \tag{5}$$

where $\Theta_{\mathrm{T}} = \det(\boldsymbol{F}_{\mathrm{T}})$ is the volume deformation due to thermal expansion. $\mathbf{1}$ is the second specific tensor.

As a kind of polymer material, the coefficient of thermal expansion (CTE) of epoxy-SMP is apparently related to temperature. We can write the volume deformation at temperature T of the material as the combination of the rubbery part and the glassy part:

$$\Theta_{\mathrm{T}}(T, T_{\mathrm{i}}, t) = 1 - \alpha_{\mathrm{r}}[T_0 - T_{\mathrm{i}}(T, t)] - \alpha_{\mathrm{g}}[T_{\mathrm{i}}(T, t) - T], \quad (6)$$

where α_{r} is the CTE of the material in the rubbery state, α_{g} is the CTE of the material in the glassy state, T_0 is the initial temperature, and T_{i} is a temperature variable related to the current temperature T and time t. We can use the internal virtual temperature T_{v} to replace the temperature variable T_{i}.T_{v} is the environmental temperature which could transform the thermal-nonequilibrium material under temperature T to be in a thermal-equilibrium state [40]. Obviously the minimum of T_{v} is T_{g}. The relationship of the internal virtual temperature T_{v} with the current temperature T can be written as

$$\frac{\mathrm{d}T_{\mathrm{v}}}{\mathrm{d}t} = -\frac{1}{\tau_{\mathrm{R}}}(T_{\mathrm{v}} - T). \quad (7)$$

For a material that is in thermal equilibrium in its initial state, the initial condition is $T_{\mathrm{v}}(T_0, t_0) = T_0$. The parameter τ_{R} denotes the structural relaxation time due to the volume creep described in the following section.

3.4. Structural relaxation

The structural relaxation of a material is expressed as the volume relaxation response to the temperature. The structural relaxation time is a variable which describes the micro-movement of the molecules within the polymer, and it is related to the viscosity, modulus, temperature, and molecular structure of the material [10, 41].

To obtain the structural relaxation time of the material in any state, we make the time–temperature shift factor of the Adam–Gibbs function equal to that of the Williams–Landel–Ferry (WLF) equation [37, 42, 43]. Then the structural relaxation time function of the material in any state is described as follows:

$$\tau_{\mathrm{R}} = \tau_{\mathrm{Rg}} \exp\left(-\frac{C_1}{\log \mathrm{e}}\left(\frac{C_2(T - T_{\mathrm{v}}) + T(T - T_{\mathrm{g}})}{T(C_2 + T_{\mathrm{v}} - T_{\mathrm{g}})}\right)\right), \quad (8)$$

where C_1 and C_2 are two material constants and $\tau_{\mathrm{Rg}} = \tau_{\mathrm{R}}\ (T_{\mathrm{g}})$ is the structural relaxation time of the material at the glass transition temperature. The constants $C_1, C_2, \tau_{\mathrm{Rg}}$ and T_{g} can be obtained through thermomechanical experiments. Specific discussion about the structural relaxation time will be presented in section 5.1.

3.5. Mechanical response: network A

The mechanical deformation of epoxy-SMP is decomposed into a hyper-elastic part and a viscoelastic part. Thus, the total strain energy can be expressed as the sum of the two parts:

$$\psi = W_{\mathrm{A}} + W_{\mathrm{B}}, \quad (9)$$

where W_{B} is the free energy of the viscoelastic part of the material and W_{A} denotes the free energy of the rubbery state of the material.

The Mooney–Rivlin function is commonly used to describe the hyper-elasticity of rubbery material [44–46]. This function is widely used in engineering due to its good applicability under medium deformation conditions. Here, we use this function to describe the rubbery state part of the material in the glass transition process:

$$W_{\mathrm{A}} = C_{10}(\lambda_1^2 + \lambda_2^2 + \lambda_3^2 - 3) + C_{01}(\lambda_1^{-2} + \lambda_2^{-2} + \lambda_3^{-2} - 3), \quad (10)$$

where C_{10} and C_{01} are two material parameters and can be determined through uniaxial tensile experiments, and the λ_{i} are stretches in the principal planar directions. For the initial state where $\lambda_1 = \lambda_2 = 1$, we have $\frac{\partial^2 W_{\mathrm{A}}}{\partial \lambda_1 \partial \lambda_2}(1, 1) = 2\mu_{\mathrm{A}}$, $C_{10} + C_{01} = \frac{1}{2}\mu_{\mathrm{A}}$, where μ_{A} is the initial shear modulus of the hyper-elastic part (network A).

Therefore, the deviator stress $\boldsymbol{\sigma}$ of the hyper-elastic part can be obtained from the Mooney–Rivlin function as follows:

$$\bar{\boldsymbol{\sigma}}_{\mathrm{A}} = \frac{2}{J}(C_{10} + I_1 C_{01})\bar{\boldsymbol{B}}_{\mathrm{M}} - \frac{2}{J}C_4\bar{\boldsymbol{B}}_{\mathrm{M}}^2, \quad (11)$$

where $\boldsymbol{B}_{\mathrm{M}} = \boldsymbol{F}_{\mathrm{M}}\boldsymbol{F}_{\mathrm{M}}^{\mathrm{T}}$ is the left Cauchy–Green deformation, I_1 is the first invariant of $\boldsymbol{B}_{\mathrm{M}}$, $J = \det(\boldsymbol{F}_{\mathrm{M}})$, and $\boldsymbol{F}_{\mathrm{M}}$ is the total mechanical deformation gradient.

3.6. Mechanical deformation response: network B

The coupling of the elastic part and the viscous part in network B can the considered as the reason for the viscoelastic deformation of the material in the glass transition process, thus the isochoric mechanical deformation gradient can also be expressed as follows:

$$\boldsymbol{F}_{\mathrm{M}} = \boldsymbol{F}_{\mathrm{e}}\boldsymbol{F}_{\mathrm{v}}, \quad (12)$$

where $\boldsymbol{F}_{\mathrm{e}}$ is the elastic deformation gradient and $\boldsymbol{F}_{\mathrm{v}}$ denotes the viscous deformation gradient.

For the elastic part in network B, in order to describe the nonlinear elastic properties of the material, the large deformation nonlinear Hencky function is considered [47–49]. The Hencky function is a revised strain energy function where the strain ε in Hooke's law is replaced by the natural logarithm of the stretch $\ln\lambda$.

We make use of the isochoric part of Hencky's strain energy function,

$$W_{\mathrm{B}} = \mu_{\mathrm{B}}(\ln \boldsymbol{U}_{\mathrm{e}}) : (\ln \boldsymbol{U}_{\mathrm{e}}), \quad (13)$$

where the elastic stretch tensor is found from the polar decomposition of the elastic deformation gradient, $\boldsymbol{F}_{\mathrm{e}} = \mathbf{R}_{\mathrm{e}}\boldsymbol{U}_{\mathrm{e}}$ with $\mathbf{R}_{\mathrm{e}}^{\mathrm{T}}\mathbf{R}_{\mathrm{e}} = \mathbf{1}$. Therefore, the deviatoric part of the Cauchy stress of network B can be determined:

$$\bar{\boldsymbol{\sigma}}_{\mathrm{B}} = \frac{2\mu_{\mathrm{B}}}{J}\mathbf{R}_{\mathrm{e}}(\ln \boldsymbol{U}_{\mathrm{e}})\mathbf{R}_{\mathrm{e}}^{\mathrm{T}}, \quad (14)$$

where $J = \det(\boldsymbol{F}_{\mathrm{M}})$. μ_{B} is the initial shear modulus of the elastic part in network B.

For viscous flow of the SMP material during the deformation process, assuming that the inelastic viscous flow is Newtonian fluid, the following relationship can be obtained [50]:

$$\dot{\gamma}_{\mathrm{v}} = -\frac{s}{\eta_{\mathrm{s}}}, \tag{15}$$

where $\dot{\gamma}_{\mathrm{v}}$ is the viscous strain rate, s is the equivalent stress of network B, $s = \left[\frac{1}{2}\bar{\boldsymbol{\sigma}}_{\mathrm{B}} : \bar{\boldsymbol{\sigma}}_{\mathrm{B}}\right]^{1/2} = \|\bar{\boldsymbol{\sigma}}_{\mathrm{B}}\|/\sqrt{2}$, and η_{s} is the viscosity of the material.

Obviously, the coefficient of viscosity of the epoxy-SMP in the vicinity of the glass transition relates to temperature. Based on Eyring's work [33], we extend the glassy viscous flowing rules for use in the glass transition process by introducing the time–temperature shift factor (section 3.4). The viscous flowing control equation in the glass transition process of the polymer can be written as follows:

$$\dot{\gamma}_{\mathrm{v}} = \frac{s_{\mathrm{y}}}{\sqrt{2}\eta_{\mathrm{sg}}}\frac{T}{Q_{\mathrm{s}}}\exp\left[-\frac{C_1}{\log \mathrm{e}}\left(\frac{C_2(T-T_{\mathrm{v}})+T(T_{\mathrm{v}}-T_{\mathrm{g}})}{T(C_2+T_{\mathrm{v}}-T_{\mathrm{g}})}\right)\right] \times \sinh\left(\frac{Q_{\mathrm{s}}}{T}\frac{s}{s_{\mathrm{y}}}\right), \tag{16}$$

where η_{sg} is the viscosity at the glass transition temperature and s_{y} is the yielding stress. Q_{s} is the active energy of the stress free state. The yielding effect of the material should not be considered if just a small deformation occurs. Then, the first order approximation of the above equation at $s = 0$ can be obtained:

$$\dot{\gamma}_{\mathrm{v}} = \frac{s_{\mathrm{y}}}{2\eta_{\mathrm{sg}}}\exp\left[-\frac{C_1}{\log \mathrm{e}}\left(\frac{C_2(T-T_f)+T(T_f-T_{\mathrm{g}})}{T(C_2+T_f-T_{\mathrm{g}})}\right)\right] \times \|\sigma^{\mathrm{neq}}\|. \tag{17}$$

As the experiments in section 2.2 show, when the material undergoes large deformation, the yielding effect or even cracks occur in the tensile test below the glass transition temperature, so the yielding and post yielding effects must be considered in the constitutive model. As discussed by Westbrook [38], the Boyce post-yielding law can be used for the yielding stress in equation (16):

$$s_{\mathrm{y}} = h\left(1 - \frac{s_{\mathrm{y}}}{s_{\mathrm{yg}}}\right), \qquad s_{\mathrm{y}}(t=0) = s_{\mathrm{y0}}, \tag{18}$$

where h is the hardening modulus of the material, s_{y0} is the yielding stress of the initial configuration, and s_{yg} is the yielding stress of the material at the glass transition temperature.

Without loss of generality, for the deformation tensor of the material, the viscous stretch rate tensor equals the viscous spatial velocity gradient if the spin rate is ignored:

$$\boldsymbol{D}_{\mathrm{v}} = \boldsymbol{L}_{\mathrm{v}}, \qquad \boldsymbol{L}_{\mathrm{v}} = \dot{\boldsymbol{F}}_{\mathrm{v}}\boldsymbol{F}_{\mathrm{v}}^{-1}, \tag{19}$$

where D_{v} is the viscous stretch rate tensor, L_{v} is the viscous spatial velocity gradient of the material, and F_{v} is the viscous deformation gradient. Recalling the previous Newton fluid assumption, the following flow equation can be obtained:

$$\boldsymbol{D}_{\mathrm{v}} = -\frac{\boldsymbol{M}}{\eta_{\mathrm{s}}}, \tag{20}$$

where $\boldsymbol{M} := \mathbf{dev}(\boldsymbol{C}_{\mathrm{e}}\mathbf{S})$ is the Mandel stress, $\boldsymbol{C}_{\mathrm{e}}$ is the right Cauchy–Green deformation tensor, $\boldsymbol{C}_{\mathrm{e}} = \boldsymbol{F}_{\mathrm{e}}^{\mathrm{T}}\boldsymbol{F}_{\mathrm{e}}$, and $\mathbf{S}$ is the second Piola-Kirchoff stress of network B, $\mathbf{S} = J_{\mathrm{e}}\boldsymbol{F}_{\mathrm{e}}^{-1}\bar{\boldsymbol{\sigma}}_{\mathrm{B}}\boldsymbol{F}_{\mathrm{e}}^{-T}$.

The differential equation that controls the viscous flowing of the material can be obtained from equations (19) and (20) as follows:

$$\dot{\boldsymbol{F}}_{\mathrm{v}} = -\frac{1}{\eta_{\mathrm{s}}}\boldsymbol{M}\boldsymbol{F}_{\mathrm{v}}. \tag{21}$$

3.7. Overview of the constitutive model

Each part of the proposed rheological model of epoxy-SMP has been established, as summarized in table 1.

The model parameters are identified through thermo-mechanical experiments in section 5.

4. Application to uniaxial tension

After inspection of the proposed constitutive equations, we found that the stress in network A is easy to obtain from the total mechanical deformation tensor, because the mechanical deformation is known in reality, while the stress in network B is difficult to obtain because the viscous deformation is controlled by a differential flowing equation. To verify the model, the uniaxial tensile state is considered. Therefore, the constitutive equations are detailed for uniaxial stress loading in order to identify all material parameters from the experiments.

For the uniaxial tensile test, the micro stress tensor is

$$\boldsymbol{\sigma} = \sigma_1 e_1 \otimes e_2, \tag{22}$$

where $\boldsymbol{\sigma}$ is the Cauchy stress. For the uniaxial tensile test, the eigenvalue of the deformation gradient tensor is the stretch λ. The micro deformation gradient is denoted as

$$\begin{aligned} &\boldsymbol{F}_{\mathrm{M}} = \lambda_1 e_1 \otimes e_2 + \lambda_2[e_2 \otimes e_2 + e_3 \otimes e_3], \\ &J = \det(\boldsymbol{F}_{\mathrm{M}}) = \lambda_1\lambda_2^2. \end{aligned} \tag{23}$$

The deviatoric part of the deformation gradient is

$$\bar{\boldsymbol{F}}_{\mathrm{M}} = \lambda e_1 \otimes e_2 + \frac{1}{\sqrt{\lambda}}[e_2 \otimes e_2 + e_3 \otimes e_3], \quad \text{where } \lambda = \left(\frac{\lambda_1}{\lambda_2}\right)^{2/3}. \tag{24}$$

Then we come to the stress in network A from equation (11). Iteration of the stress in network A is obtained as follows:

$$(\bar{\boldsymbol{\sigma}}_{\mathrm{A}})^n = \frac{2}{J^n}(C_{10} + I_1^n C_{01})(\bar{\boldsymbol{B}}_{\mathrm{M}})^n - \frac{2}{J^n}C_{01}(\bar{\boldsymbol{B}}_{\mathrm{M}}^2)^n, \tag{25}$$

where $(\boldsymbol{B}_{\mathrm{M}})^n = (\boldsymbol{F}_{\mathrm{M}})^n(\boldsymbol{F}_{\mathrm{M}}^{\mathrm{T}})^n$ and $J^n = \det(\boldsymbol{F}_{\mathrm{M}}^n)$.

The hydrostatic pressure iteration can also be obtained as follows:

$$p^n = 3k\frac{\ln J^n}{J^n}, \tag{26}$$

Table 1. The thermo-viscoelastic constitutive model of epoxy-SMP.

Stress response: $\boldsymbol{\sigma} = \bar{\boldsymbol{\sigma}}_{\mathrm{A}} + \bar{\boldsymbol{\sigma}}_{\mathrm{B}} + p\mathbf{1}$, where
$\bar{\boldsymbol{\sigma}}_{\mathrm{A}} = \frac{2}{J}(C_{10} + I_1 C_{01})\bar{\boldsymbol{B}}_{\mathrm{M}} - \frac{2}{J} C_{01}\bar{\boldsymbol{B}}_{\mathrm{M}}^2$
$\bar{\boldsymbol{\sigma}}_{\mathrm{B}} = \frac{2\mu_{\mathrm{B}}}{J}\mathbf{R}_{\mathrm{B}}^{e}(\ln \boldsymbol{U}_{\mathrm{B}}^{e})\mathbf{R}_{\mathrm{B}}^{et}$
$p = 3k\frac{\ln J}{J}$, $J = \det(\boldsymbol{F}_{\mathrm{M}})$
Deformation: $\boldsymbol{F} = \boldsymbol{F}_{\mathrm{T}}\boldsymbol{F}_{\mathrm{e}}\boldsymbol{F}_{\mathrm{v}}$, where
$\boldsymbol{F}_{\mathrm{T}} = \Theta_{\mathrm{T}}^{1/3}\mathbf{1}$, $\Theta_{\mathrm{T}}(T, T_f) = 1 - \alpha_{\mathrm{r}}(T_0 - T_{\mathrm{v}}) - \alpha_{\mathrm{g}}(T_{\mathrm{v}} - T)$
$\dot{\boldsymbol{F}}_{\mathrm{v}} = -\frac{1}{\eta_{\mathrm{s}}}\boldsymbol{M}\boldsymbol{F}_{\mathrm{v}}$, $\eta_{\mathrm{s}} = -\frac{s}{\dot{\gamma}_{\mathrm{v}}}$ with
$\dot{\gamma}_{\mathrm{v}} = \frac{s_{\mathrm{y}}}{2\eta_{\mathrm{sg}}}\exp\left[-\frac{C_1}{\log \mathrm{e}}\left(\frac{C_2(T-T_{\mathrm{v}})+T(T_{\mathrm{v}}-T_{\mathrm{g}})}{T(C_2+T_{\mathrm{v}}-T_{\mathrm{g}})}\right)\right]\|\bar{\boldsymbol{\sigma}}_{\mathrm{B}}\|$, $s = \left[\frac{1}{2}\bar{\boldsymbol{\sigma}}_{\mathrm{B}} : \bar{\boldsymbol{\sigma}}_{\mathrm{B}}\right]^{1/2}$

where k is the bulk modulus of epoxy-SMP, and is obtained from the total shear modulus $\mu = \mu_{\mathrm{A}} + \mu_{\mathrm{B}}$ and Poisson ratio ν

$$k = \frac{2\mu(1+\nu)}{3(1-2\nu)}. \tag{27}$$

The nonequilibrium stress is more complicated because the viscous deformation of the initial state is unknown except for the elastic deformation. Therefore, the nonequilibrium stress is updated by updating the elastic deformation tensor.

From equations (19)–(21), the relationship between the elastic deformation and the viscous deformation can be obtained as follows:

$$\boldsymbol{F}_{\mathrm{e}}\boldsymbol{L}_{\mathrm{v}}\boldsymbol{F}_{\mathrm{e}}^{\mathrm{T}} = -\frac{\boldsymbol{B}_{\mathrm{e}}\bar{\boldsymbol{\sigma}}_{\mathrm{B}}}{\eta_{\mathrm{s}}}. \tag{28}$$

To solve the nonlinear viscous flowing equation, the backward Euler updating algorithm [51] of the left Cauchy–Green deformation tensor can be obtained by using equation (28) as follows:

$$\frac{1}{2}\ln \boldsymbol{B}_{\mathrm{e}}^{n+1} + \frac{\Delta t}{\eta_{\mathrm{s}}}(\bar{\boldsymbol{\sigma}}_{\mathrm{B}})^{n+1} - \frac{1}{2}\ln \boldsymbol{B}_{\mathrm{trial}} = 0, \tag{29}$$

where $\boldsymbol{B}_{\mathrm{trial}} = (\boldsymbol{F}^{n+1})(\boldsymbol{C}_{\mathrm{v}}^{n})^{-1}(\boldsymbol{F}^{n+1})^{\mathrm{T}} = (\boldsymbol{F}^{n+1})(\boldsymbol{F}^{n})^{-1}\boldsymbol{B}_{\mathrm{e}}^{n}(\boldsymbol{F}^{n})^{-T}(\boldsymbol{F}^{n+1})^{\mathrm{T}}$ is the coupling term between the nth step and the $(n+1)$th step of the left Cauchy–Green deformation tensor.

As previously mentioned, the stress tensor of network B at the nth step obtained from the Hencky model is

$$(\sigma_{\mathrm{B}})^{n} = 2\mu_{\mathrm{B}}\ln(\boldsymbol{B}_{\mathrm{e}}^{n})^{1/2}. \tag{30}$$

Substituting equation (30) into equation (29), the left Cauchy–Green deformation tensor can be obtained as follows:

$$\left(1 + \frac{2\mu_{\mathrm{B}}\Delta t}{\eta_{\mathrm{s}}^{n+1}}\right)\ln \boldsymbol{B}_{\mathrm{e}}^{n+1} = \ln((\boldsymbol{F}^{n+1})(\boldsymbol{F}^{n})^{-1} \times \boldsymbol{B}_{\mathrm{e}}^{n}(\boldsymbol{F}^{n})^{-T}(\boldsymbol{F}^{n+1})^{\mathrm{T}}), \tag{31}$$

where the initial condition is $\boldsymbol{B}_{\mathrm{e}}(t=0) = \boldsymbol{I}$.

Therefore, the iteration of the total stress of the constitutive model can be obtained as

$$\sigma^{n} = (\bar{\sigma}_{\mathrm{B}})^{n} + (\bar{\sigma}_{\mathrm{A}})^{n} + p^{n}. \tag{32}$$

5. Determination of the epoxy-SMP material parameters

To obtain the material parameters in the proposed model, some experiments were performed and then simulated. The model was implemented in a User Subroutines code.

5.1. Thermal expansion model

Using the thermal expansion model to simulate and fit the thermal expansion experiment, the parameters in the thermal expansion model can be determined. The thermal strain of epoxy-SMP in the cooling process from 120 to 60 °C is considered. The time–temperature shift factor in section 3.3 is defined as $ek = \exp\left(-\frac{C_1}{\log \mathrm{e}}\left(\frac{C_2(T-T_{\mathrm{v}})+T(T-T_{\mathrm{g}})}{T(C_2+T_{\mathrm{v}}-T_{\mathrm{g}})}\right)\right)$. Then, the relationships of the time–temperature shift factor versus temperature and the virtual variable versus temperature can be obtained as shown in figure 5.

As shown in figure 5, there is a large mutation around the glass transition temperature for both the time–temperature shift factor and the virtual variable T_{v}. The time–temperature shift factor is very large at low temperature, resulting in a long structural relaxation time, and more time is needed for the material to reach the equilibrium state. The time–temperature shift factor is small in the high-temperature range and therefore results in a shorter structural relaxation time for the material to reach the equilibrium state. The thermal expansion model can describe the epoxy-SMP structural relaxation phenomenon in the vicinity of the glass transition temperature nicely. It can also be seen that the glass transition temperature is the limiting value of the internal variable temperature. The equilibrium temperature of the material at high temperature is just the initial environmental temperature, while the equilibrium temperature of the material at low temperature is the glass transition temperature.

The thermal expansion is simulated as shown in figure 6. The thermal expansion model parameters can be obtained through the simulation by using the CTEs of the glassy and rubbery states and the glass transition temperature. The model parameter C_1 is always chosen as 17.44 for amorphous polymers [37]; therefore, we can obtain $C_2 = 85\,^{\circ}\mathrm{C}$, $\tau_{\mathrm{Rg}} = 20$ s.

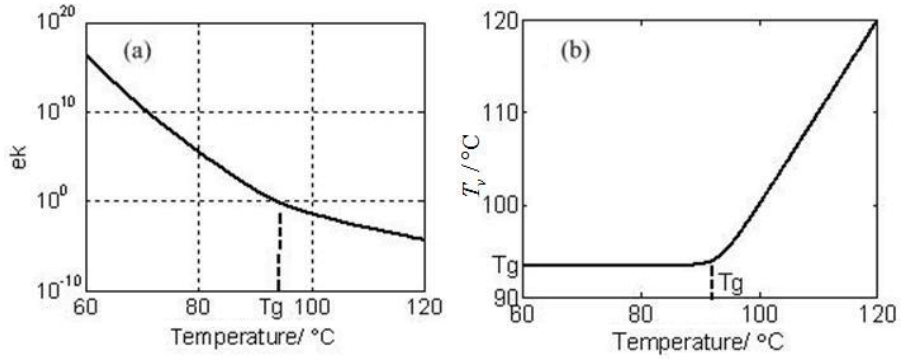

Figure 5. The time–temperature shift factor (a) and the internal variable T_v (b).

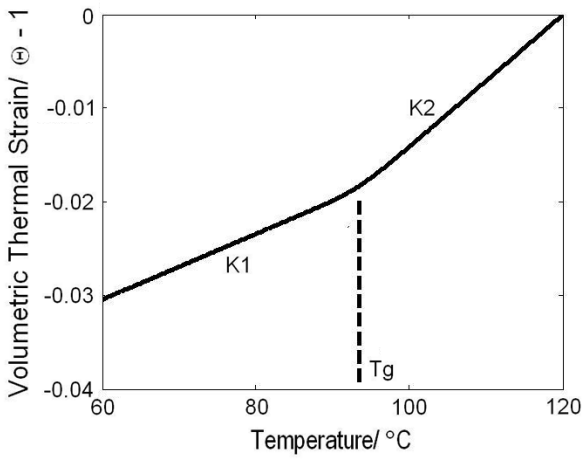

Figure 6. Thermal expansion simulation of epoxy-SMP.

5.2. DMA simulation

The DMA experiment can characterize the viscoelasticity of the material, thus we can obtain the viscosity information through simulation of the DMA experiment. A dynamic displacement load is applied in the simulation; the nominal strain amplitude is 0.005, the frequency is 1 Hz, thus the vibration strain is $\varepsilon_{\text{nom}} = 0.005\sin(2\pi \cdot t)$; the simulation temperature range is 70–120 °C. As epoxy-SMP is a viscoelastic material, the stress to strain lag phase is δ, $\delta = 2\pi f \cdot \Delta$, where Δ is the lag time and f is the frequency. The DMA test is simulated without considering the yielding effect because the material only undergoes small deformation. The DMA simulation result is shown in figure 7.

The simulation result for $\eta_{\text{sg}} = 2 \times 10^7$ Pa s^{-1} gives the best fitting to the experiment.

5.3. Uniaxial tensile test

The initial shear moduli of network A and network B are determined through the uniaxial tensile test at temperatures of $T > T_g + 20$ K and $T < T_g - 20$ K respectively. Room temperature (22 °C) and high temperature (120 °C) are chosen for the experiments (as shown in figure 8). The initial linear range of the test figure is chosen to obtain the initial modulus. It can be determined that the initial Young's moduli of epoxy-SMP are $E_{0g} = 2.16$ GPa and $E_{0r} = 12.89$ MPa for the glassy and rubbery states, which agree well with the DMA test values of 2.03 GPa (25 °C) and 13 MPa (120 °C).

Suppose that the Poisson's ratios of epoxy-SMP are the same as those of a typical amorphous polymer material [48], that is a glassy state with $\nu_g = 0.35$ and a rubbery state with $\nu_r = 0.5$. As the linear elastic initial state equation is $\mu = \frac{E_0}{2(1+\nu)}$, the shear moduli in networks A and B can be obtained as $\mu_A = 4.30$ MPa and $\mu_B = 800$ MPa. The Mooney–Rivlin model constants are obtained by fitting the uniaxial tensile test data (120 °C) of epoxy-SMP, so we get $C_{01} = -8.20 \times 10^7$ Pa, $C_{10} = 8.42 \times 10^7$ Pa. The initial shear modulus in network A can also be determined as $C_{01} + C_{10} = \mu_A/2$, $\mu_A = 4.4$ MPa. The other model parameters are obtained by simulation of the uniaxial tension test of epoxy-SMP at 80 °C at a strain rate of 0.33×10^{-2} s^{-1}; the fitting result is shown in figure 9. The simulation yields the yielding stress in the initial state $s_{y0} = 10^8$ Pa, the yielding stress at the glass transition temperature $s_{ys} = 35 s_{y0}$, the active energy of the stress free state $Q_s = 1.8 \times 10^3$ J, and the strain hardening modulus $h = 800$ MPa. Finally, all the model parameters are determined as shown in table 2.

6. Verification of the constitutive model

We will compare the mechanical test data with the numerical simulation results under different conditions to verify the proposed model. The subsequent experiments are isothermal uniaxial tensile experiments under different temperature conditions and thermodynamic cycle experiments.

Before the verification, recall that the viscosity in equation (16) also involves the time–temperature shift factor (section 5.1), therefore we can explain the shape memory effect of epoxy-SMP from this perspective through our proposed constitutive model. For SMP at high temperature, the molecular chains move extensively, meaning that the molecular structure can quickly relax to reach an equilibrium state to adapt to environmental temperature changes, so that the viscosity of the material (describing the amount of micro-molecular motion of the material) becomes low, and changes instantly with temperature. If it is cooled at this time after deformation, the time to reach the equilibrium state will be very long because

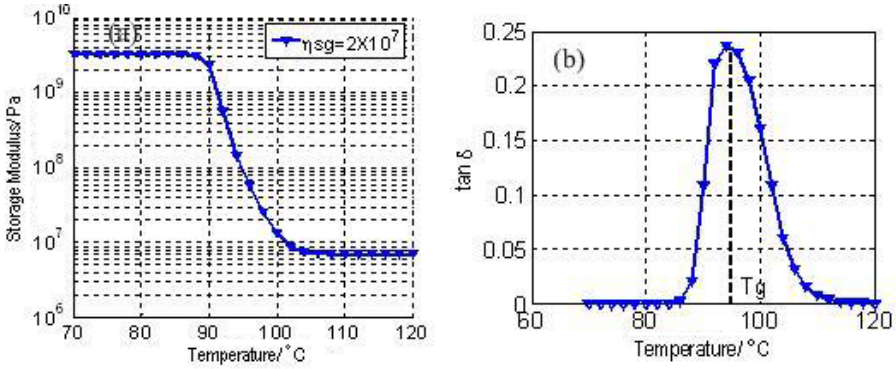

Figure 7. Simulation of the DMA test: storage modulus (a) and loss angle (b).

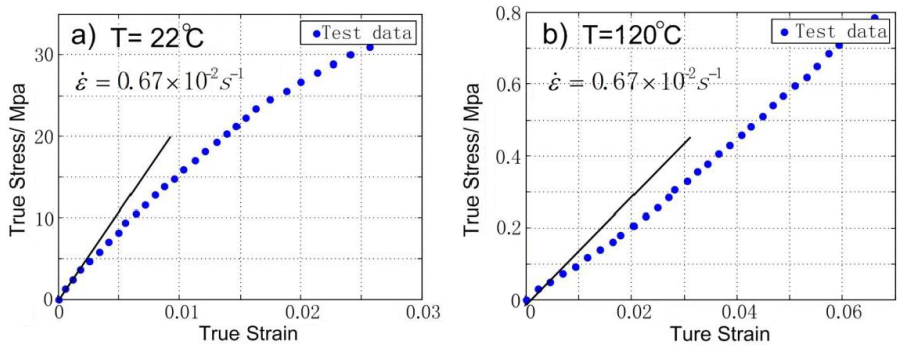

Figure 8. Mechanical properties of epoxy-SMP at temperatures of 22 °C (a) and 120 °C (b) with a strain rate of 0.67×10^{-2} s^{-1}.

Table 2. Model parameters of epoxy-SMP.

Parameter	Value	Physical meaning
α_g	1.17×10^{-4} °C^{-1}	CTE of glassy state
α_r	2.35×10^{-4} °C^{-1}	CTE of rubbery state
T_g	92.17 °C	Glass transition temperature
η_{sg}	2×10^7 Pa s^{-1}	Viscosity in glassy state
μ_A	4.30 MPa	Initial shear modulus of network A
μ_B	800 MPa	Initial shear modulus of network B
C_{10}	-8.20×10^7 Pa	Mooney–Rivlin model constant
C_{01}	8.42×10^7 Pa	Mooney–Rivlin model constant
s_{y0}	10^8 Pa	Yielding stress in initial state
s_{yg}	$35s_{y0}$	Yielding stress at T_g
Q_s	1.8×10^3 J	Active energy of the stress free state
h	800 MPa	Strain hardening modulus
C_1	17.44	WLF parameter
C_2	85 °C	WLF parameter
τ_{Rg}	20 s	Structural relaxation time at T_g

of the sharp reduction of the heat energy and the slowing down of the molecular movement of the molecular chain; this nonequilibrium state results in storage of the strain energy of the material. When reheated to above the glass transition temperature, the molecular chains move extensively again, so that the material quickly reaches an equilibrium state, thus expressing the shape recovery of the material.

6.1. Mechanical properties under thermal field

The isothermal uniaxial tensile tests at different temperatures and different strain rates are simulated through the proposed constitutive model, the yielding model (equation (18)) is used in the simulation, and finally the simulation results are presented in figure 9.

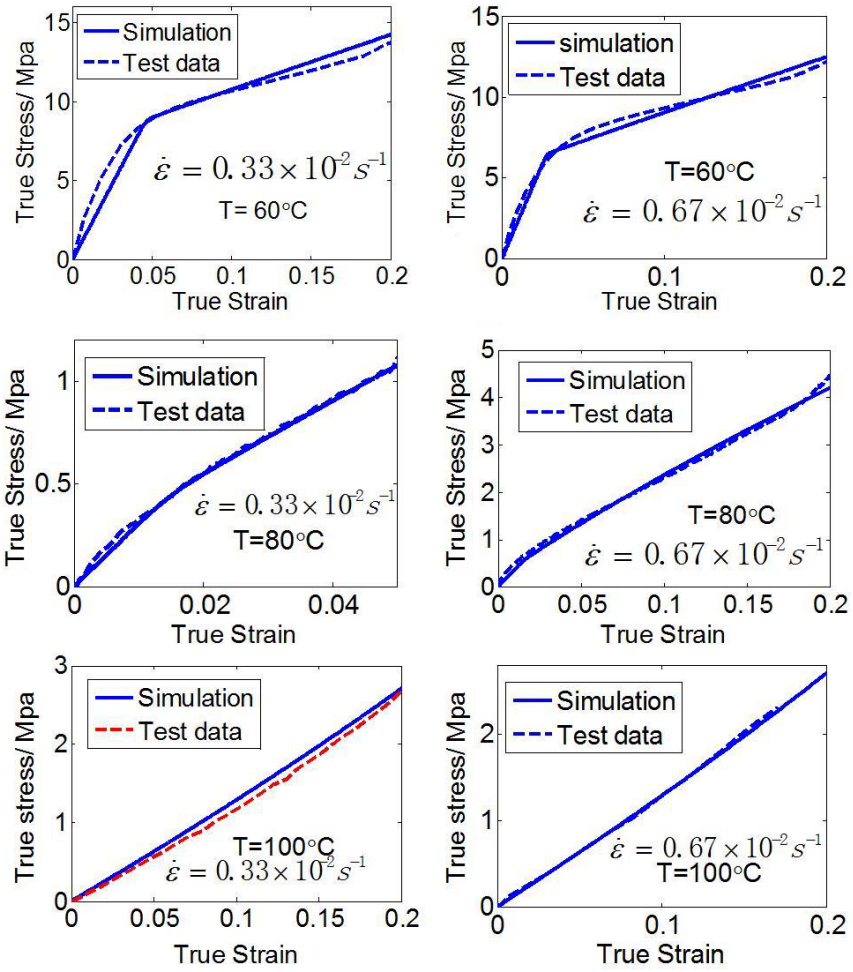

Figure 9. Simulations of the uniaxial tensile tests: the temperature conditions are 60, 80 and 100 °C and the strain rates are 0.33×10^{-2} s^{-1} and 0.67×10^{-2} s^{-1}.

It can be seen from the comparison between the test data and the simulation data that the simulation results agree well with the test results. The developed constitutive model can explain well the simple static mechanical properties of epoxy-SMP in the isothermal uniaxial tensile test such as the yielding effect, the influence of different strain rates on the stress of the material, and the different mechanical performance below and above the glass transition temperature.

6.2. Mechanical properties of the thermo-mechanical cycle experiments

For further verification of the proposed constitutive model, a more complicated thermomechanical test is conducted. The thermomechanical cycle test is executed, and the test process is as follows: stretch the sample to reach a certain strain (e.g. 10%) under high temperature conditions (120 °C); the environmental temperature undergoes a cycle from high to low and then to high under the condition that the displacement is kept constant; the temperature and the reaction force of the sample's ends are measured throughout the whole procedure. Figure 10 shows the test curve.

The thermomechanical cycle test is simulated by using the experimentally measured temperature change and strain change as the input of the simulation. The stress changes are detected in the simulation and then compared with the experimental data.

The temperature is maintained after the sample is stretched to about 4.5% strain. Epoxy-SMP shows a stress relaxation effect like a typical polymer material (the stress decreases while the strain remains unchanged). The stress reaches a steady level after about 10 min of maintaining the load, then the temperature decreases to below the glass transition temperature, 36 °C, under the condition that the strain is still maintained. As a consequence of the contraction due to the decrease of the thermal strain and the constraints due to the clamps between the sample's ends, there is a stretch between the sample and the clamps, which results in a stress increase in the cooling process. The constraint force reaches a maximum when the temperature decreases to its lowest level (at about 1000 s). Soon afterwards, the SME of epoxy-SMP is frozen in the cooling process, which results in a sharp decrease of the stress. When the temperature increases again, the stress decreases sharply due to the relaxation, which is a result of the thermal expansion between the sample and the clamps.

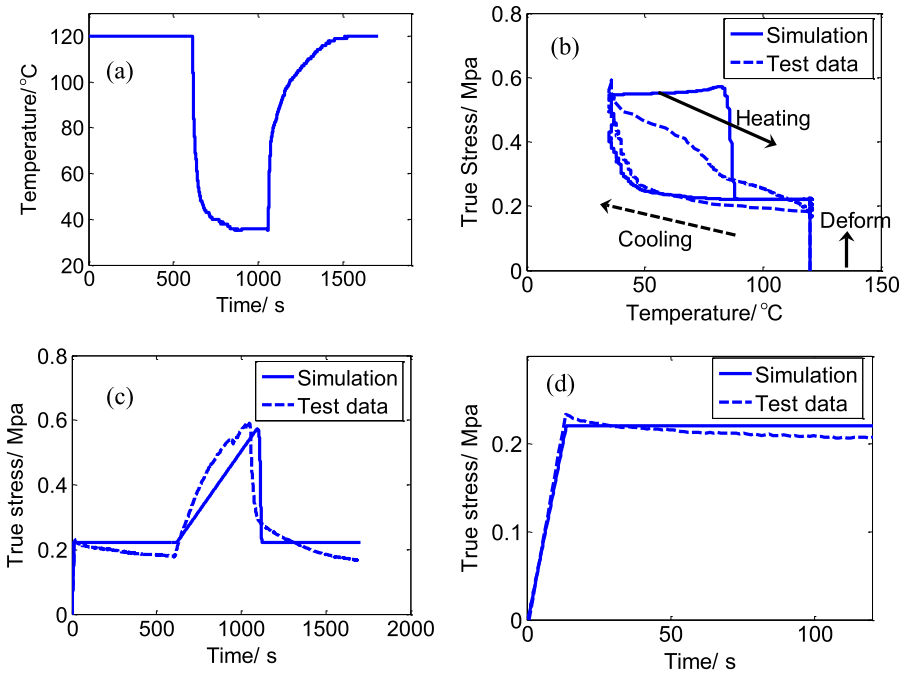

Figure 10. Thermomechanical cycle test: (a) temperature changes with time, (b) true stress changes with temperature, (c) true stress changes with time, (d) true stress changes with time in the stretching stage.

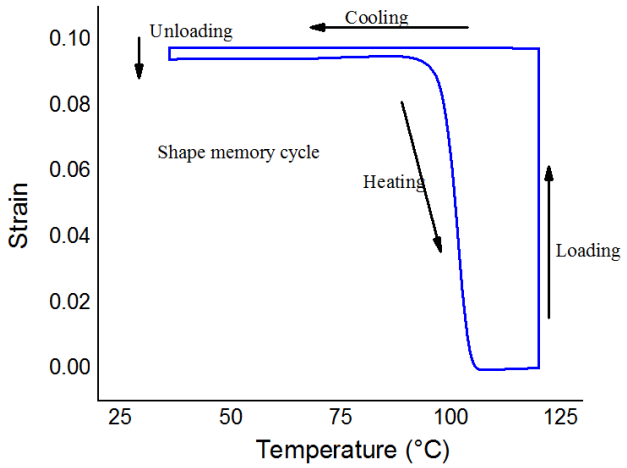

Figure 11. Predicted shape memory cycle.

In the predicted shape memory cycle, the strain increases in the loading process when the material is in the rubbery state, and then the strain is maintained in the cooling process, where after the small elastic strain recovers, the whole shape is temporarily fixed. On heating back to high temperature, the strain maintained in the material is totally released; this results in shape restoration, and we can see that the strain is released rapidly around the glass transition region, as shown in figure 11.

The proposed method can effectively describe the complex mechanical properties of epoxy-SMP such as the stress changes with time in the thermomechanical cycle test, especially in the stretching stage and the frozen stage. The model can also predict well the stress changes with temperature of epoxy-SMP in the thermomechanical cycle test and can clearly predict shape memory behavior.

7. Conclusion

A rheological constitutive model based on a revised standard linear solid (SLS) element and a thermal expansion element is proposed for SMP material by considering the structural relaxation and viscoelastic properties to characterize the mechanical behavior of epoxy-SMP. Then, verification of the model is conducted through various experiments. Analysis of the experimental data shows a nonlinear viscoelastic and thermal effect of the material. The model is used to predict the measured stress–strain–temperature curves for various loading histories. The results show that the constitutive model can forecast the response under different temperature and loading conditions well. Furthermore, the model predictions of the thermomechanical cycle agree with the experiments, but most importantly the proposed method can clearly predict the shape memory behavior of SMP and is very useful for the design of SMP structures.

Acknowledgment

This work is supported by the National Natural Science Foundation of China (Grant Nos 11225211, 11272106, 11102052).

References

[1] Leng J, Lan X, Liu Y and Du S 2010 Shape-memory polymers and their composites: stimulus methods and applications *Prog. Mater. Sci.* **56** 1077–135

[2] Behl M and Lendlein A 2007 Shape-memory polymers *Mater. Today* **10** 20–8

[3] Liu Y J, Lv H B, Lan X, Leng J S and Du S Y 2009 Review of electro-activate shape-memory polymer composite *Compos. Sci. Technol.* **69** 2064–8

[4] Ratna D and Karger-Kocsis J 2008 Recent advances in shape memory polymers and composites: a review *J. Mater. Sci.* **43** 254–69

[5] Liu Y J, Du H Y, Liu L W and Leng J S 2014 Shape memory polymer composites and their applications in aerospace: a review *Smart Mater. Struct.* **23** 023001

[6] Wei Z G, Sandstrom R and Miyazaki S 1998 Shape-memory materials and hybrid composites for smart systems. I. Shape-memory materials *J. Mater. Sci.* **33** 3743–62

[7] Tan Q, Liu L W, Liu Y J and Leng J S 2013 Post buckling analysis of a shape memory polymer composite laminate with a built-in stiff film *Composites* B **53** 218–25

[8] Yakacki C M, Shandas R, Lanning C, Rech B, Eckstein A and Gall K 2007 Unconstrained recovery characterization of shape-memory polymer networks for cardiovascular applications *Biomaterials* **28** 2255–63

[9] Liu Y P, Gall K, Dunn M L, Greenberg A R and Diani J 2006 Thermomechanics of shape memory polymers: uniaxial experiments and constitutive modeling *Int. J. Plast.* **22** 279–313

[10] Lendlein A and Kelch S 2002 Shape-memory polymers *Angew. Chem. Int. Edn Engl.* **41** 2035–57

[11] Mather P T, Luo X and Rousseau I A 2009 Shape memory polymer research *Annu. Rev. Mater. Res.* **39** 445–71

[12] Lan X, Liu L W, Liu Y J, Leng J S and Du S Y 2014 Microbuckling mechanics of fiber-reinforced shape-memory polymer composite *Mech. Mater.* **72** 46–60

[13] Liu Y, Gall K, Dunn M L and McCluskey P 2004 Thermomechanics of shape memory polymer nanocomposites *Mech. Mater.* **36** 929–40

[14] Schmidt A M 2006 Electromagnetic activation of shape memory polymer networks containing magnetic nanoparticles *Macromol. Rapid Commun.* **27** 1168–72

[15] Mohr R, Kratz K, Weigel T, Lucka-Gabor M, Moneke M and Lendlein A 2006 Initiation of shape-memory effect by inductive heating of magnetic nanoparticles in thermoplastic polymers *Proc. Natl Acad. Sci. USA* **103** 3540–5

[16] Jiang H Y, Kelch S and Lendlein A 2006 Polymers move in response to light *Adv. Mater.* **18** 1471–5

[17] Lendlein A, Jiang H, Junger O and Langer R 2005 Light-induced shapememory polymers *Nature* **434** 879–82

[18] Scott T F, Draughon R B and Bowman C N 2006 Actuation in crosslinked polymers via photoinduced stress relaxation *Adv. Mater.* **18** 2128–32

[19] Li M H, Keller P, Li B, Wang X and Brunet M 2003 Light-driven sideon nematic elastomer actuators *Adv. Mater.* **15** 569–72

[20] Cho J W, Kim J W, Jung Y C and Goo N S 2005 Electroactive shape-memory polyurethane composites incorporating carbon nanotubes *Macromol. Rapid Commun.* **26** 412–6

[21] Zhang L, Du H Y, Liu L W, Liu Y J and Leng J S 2014 Analysis and design smart mandrels using shape memory polymers *Composites* B **59** 230–7

[22] Lendlein A and Langer R 2002 Biodegradable, elastic shape-memory polymers for potential biomedical applications *Science* **296** 1673–6

[23] Yu K, Liu Y J and Leng J S 2011 Conductive shape memory polymer composite incorporated with hybrid fillers: electrical, mechanical, and shape memory properties *J. Intell. Mater. Syst. Struct.* **22** 369–79

[24] Behl M and Lendlein A 2007 Actively moving polymers *Soft Matter* **3** 58–67

[25] Hayashi S, Tobushi H and Kojima S 1992 Mechanical properties of shape memory polymer of polyurethane series: basic characteristics of stress–strain–temperature relationship *JSME Int. J. Ser. 1, Solid Mech. Strength Mater.* **35** 296–302

[26] Miaudet P, Derre A, Mauyse M, Zakri C, Piccione P M, Inoubli R and Poulin P 2007 Shape and temperature memory of nanocomposites with broadened glass transition *Science* **318** 1294–6

[27] Tobushi H and Hashimoto T 1997 Thermomechanical constitutive modeling in shape memory polymer of polyurethane series *J. Intell. Mater. Syst. Struct.* **8** 711–8

[28] Tobushi H, Okumura K and Hayashi S 2001 Thermomechanical constitutive model of shape memory polymer *Mech. Mater.* **33** 545–54

[29] Diani J, Liu Y and Gall K 2006 Finite strain 3D thermoviscoelastic constitutive model for shape memory polymers *Polym. Eng. Sci.* **46** 486–92

[30] Chen Y and Lagoudas D C 2008 A constitutive theory for shape memory polymers. Part I: large deformations *J. Mech. Phys. Solids* **56** 1752–65

[31] Chen Y and Lagoudas D C 2008 A constitutive theory for shape memory polymers. Part II: a linearized model for small deformations *J. Mech. Phys. Solids* **56** 1766–78

[32] Barot G, Rao I J and Rajagopal K R 2008 A thermodynamic framework for the modeling of crystallizable shape memory polymers *Int. J. Eng. Sci.* **46** 325–51

[33] Leng J, Wu X and Liu Y 2009 Effect of a linear monomer on the thermomechanical properties of epoxy shape-memory polymer *Smart Mater. Struct.* **18** 095031

[34] Yu K, Xie T, Leng J, Ding Y and Qi H J 2012 Prediction of temperature-dependent free recovery behaviors of amorphous shape memory polymers *Soft Matter* **8** 11098–105

[35] Ge Q, Yu K, Ding Y and Qi H J 2012 Prediction of temperature dependent free recovery behaviors of shape memory polymers *Soft Matter* **8** 11098–105

[36] Yu K, Ge Q and Qi H J 2014 Reduced time as a unified parameter determining fixity and free recovery of shape memory polymers *Nature Commun.* **5** 3066

[37] Nguyen T D, Qi J H and Castro F 2008 A thermoviscoelastic model for amorphous shape memory polymers: incorporating structural and stress relaxation *J. Mech. Phys. Solids* **56** 2792–814

[38] Westbrook K K, Kao P H and Castro F 2011 A 3D finite deformation constitutive model for amorphous shape memory polymers: a multi-branch modeling approach for nonequilibrium relaxation processes *Mech. Mater.* **43** 853–69

[39] Qi H J and Boyce M C 2005 Stress–strain behavior of thermoplastic polyurethanes *Mech. Mater.* **37** 817–39

[40] Tool A Q 1946 Viscosity and extraordinary heat effects in glass *J. Res. Natl. Bur. Stand.* **37** 74–90

[41] Lendlein A and Kelch S 2002 Shape-memory polymers *Angew. Chem. Int. Edn* **41** 2034–57

[42] Wineman A S and Rajagopal K R 2000 *Mechanical Response of Polymers: An Introduction* (Cambridge: Cambridge University Press) pp 40–2

[43] Williams M L, Landel R F and Ferry J D 1955 The temperature dependence of relaxation mechanisms in

amorphous polymers and other glass-forming liquids *J. Am. Chem. Soc.* **77** 3701–7
[44] Liu Y, Liu L, Leng J, Yu K and Sun S 2009 Electromechanical stability of dielectric elastomer *Appl. Phys. Lett.* **94** 211901
[45] Liu Y, Liu L, Shi L, Sun S and Leng J 2009 Comment on 'On electromechanical stability of dielectric elastomers' *Appl. Phys. Lett.* **94** 096101
[46] Liu Y, Liu L, Zhang Z, Shi L and Leng J 2008 Comment on 'Method to analyze electromechanical stability of dielectric elastomers' *Appl. Phys. Lett.* **93** 106101
[47] Hayes M and Saccomandi G 2002 *Topics in Finite Elasticity* (Berlin: Springer) pp 40–157
[48] Xiao H and Chen L S 2002 Hencky's elasticity model and linear stress–strain relations in isotropic finite hyperelasticity *Acta Mech.* **157** 51–60
[49] Horgan C O and Murphy J G 2009 A generalization of Hencky's strain–energy density to model the large deformations of slightly compressible solid rubbers *Mech. Mater.* **41** 943–50
[50] Holzapfel G A 1999 *Nonlinear Solid Mechanics: A Continuum Approach for Engineering* (New York: Wiley) pp 286–9
[51] Reese S and Govindjee S 1998 A theory of finite viscoelasticity and numerical aspects *Int. J. Solids Struct.* **35** 3455–82